

# SIMULATIONS OF HIGH-PRESSURE SUBCOOLED BOILING FLOWS IN RECTANGULAR CHANNELS

**R. Thakrar<sup>1</sup>, J. Murallidharan, and S.P. Walker**  
Imperial College London, Department of Mechanical Engineering  
Exhibition Road, London, SW7 2AZ, UK  
rkt08@imperial.ac.uk; j.murallidharan@imperial.ac.uk

## ABSTRACT

Subcooled boiling flows are commonplace in the nuclear industry. Computational Fluid Dynamics (CFD) is now beginning to be used to deliver the relevant two-phase thermal hydraulic analyses required for nuclear applications. This paper presents a blind assessment of the capabilities of the commercial CFD code STAR-CCM+ against the measurements for a vertically upward subcooled boiling flow in a uniformly-heated rectangular channel at a pressure of over 40 bar. The reported measurements comprised distributions of the transverse line-averaged void at a large number of axial locations; an estimate of the axial profile of the overall flow-area or cross-sectionally averaged void could also be derived from these measurements. The predictive ability of several combinations of turbulence, wall heat flux partitioning and interfacial area transport models was tested. In general, good agreement was obtained for the area-averaged void, with the most mechanistic modelling combination reproducing the measurements accurately. Reasonable agreement was also observed for the distributions of transverse void, however this agreement could not be maintained beyond the entrance of the channel. The prediction of the transition from near-wall void peak to core void peak exhibited in the experiments could not be reproduced accurately with any of the considered modelling combinations, although the basic qualitative trend was partly captured. Suggestions for future investigation are outlined subsequently.

## KEYWORDS

Subcooled flow boiling, high-pressure, rectangular geometry, CFD

## 1. INTRODUCTION

Subcooled boiling often arises in industrial processes that drive substantial rates of heat transfer. Almost all water-cooled nuclear reactors experience some degree of subcooled boiling during normal operation as well as partially under fault conditions. Most commercial CFD codes now integrate some degree of modelling capability and the application of these codes towards the prediction of industrial-scale boiling two-phase flows of water at high-pressure have been widely reported in the academic literature over the past decade. At high-pressure, code validation concentrates predominantly against a narrow set of measurable ‘aggregate’ or ‘macroscopic’ flow field information; the distribution of void is of particular interest in thermal hydraulic analyses and is measured frequently in experimental investigations at high pressure. Most CFD activities have focused on flows in circular geometries, for which data is most readily available. Perhaps the simplest and most extensively investigated [1] high-pressure case is that of Bartolomei et al. [2] who recorded measurements of the axial profile of area-averaged void for a turbulent upwards flow of water in a heated tube at pressures above 40 bar. Limited benchmarking activities have been reported more recently against measurements of the area-averaged void in non-circular reactor-prototypic rod-bundle / subchannel type geometries [3, 4].

Whilst multi-dimensional CFD analyses hold the potential to capture the boiling phenomenon in greater detail than the conventional approaches used in the nuclear industry, the majority of the required constitutive relations continue to rely heavily on empirical expressions (albeit containing some first-

principles justifications) that were developed originally toward application in one-dimensional analyses. It is often the case that substantial adjustment, calibration or ‘tuning’ of the various parameters that comprise these constitutive relations is required in order to extend code capability towards the particular case of interest [5]. Consequently, it is not unusual for benchmarking to resemble an iterative process that is aided somewhat by detailed knowledge of the investigated case rather than true ‘blind’ prediction.

In the present work, the capability of the general-purpose commercial CFD code STAR-CCM+ (v9.04) is assessed against the measurements of Pierre and Bankoff [6, 7] for a vertically upward subcooled boiling flow of water in a uniformly-heated rectangular channel at 41 bar. In addition to detailing the area-averaged void at various axial locations along the channel, the selected data set also provides valuable information regarding the void distribution across the flow area at each measured location. In order to assess blind performance, the CFD analysis is undertaken ‘as is’, that is, with several pre-selected combinations of models, each representing different default configurations of the code without user calibration. The selected combinations enable the influence of three distinct modelling components to be examined: continuous-phase turbulence, wall boiling and interfacial area transport (IAT).

## 2. The Investigated Experiment

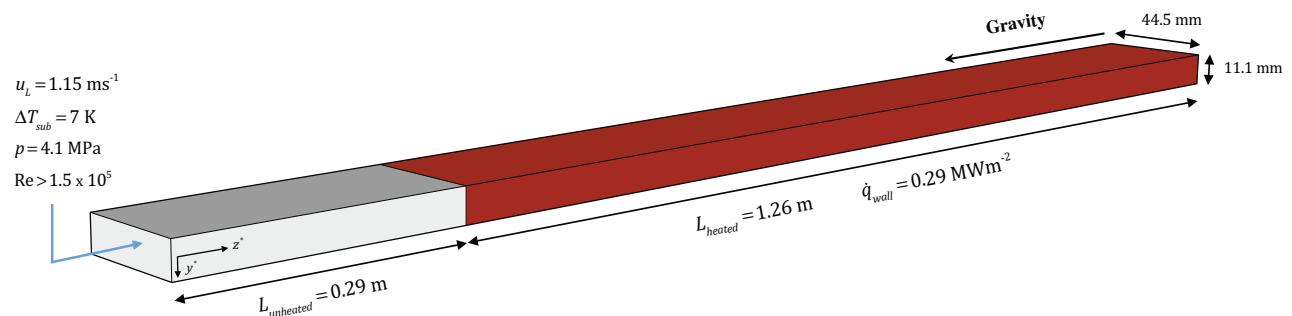


**Fig 1. Schematic of the test section and experimental conditions**

The test section assembly, illustrated in Figure 1, comprises a vertical thermally-insulated straight rectangular channel fabricated from Type 304 stainless steel through which water is pumped upwards. The channel has a total length of 1.55 m and a flow area of 11.1 x 44.5 mm. All four walls of the channel are heated electrically and uniformly beginning 0.29 m from the entrance for a length of 1.26 m. Steam generated in the test section is bled off in a separator that follows the test section and water (combined with make-up water to replenish the bleed) is re-circulated to the test section at a controlled pressure, temperature and flow rate. A supplementary ‘transition piece’ of length 0.64 m of the same dimensions as the test section precedes the illustrated test section so as to eliminate any lingering pockets of void at the entrance and to provide a smooth flow transition from the return leg to the entrance of the test section.

A gamma-ray attenuation technique driven by a Thulium-170 pellet source is utilized for the measurement of the average flow density, which is then converted into an estimate for the void fraction. The void-detection system employs a pair of 0.8 mm collimating windows that are aligned on the either side of the test section along the 11.5 mm narrow or ‘transverse’ width, which constrain the beam to a thin cross section. The collimator-pair can be traversed both horizontally and vertically across the transverse width and could be used to obtain, in effect, ‘point-wise’ measurements of the line-averaged void at any location along the transverse width (in which the gamma beam is passed through the entirety of the 44.5 mm channel depth or longitudinal width). Measurements were taken at multiple points along the transverse width at thirteen equidistantly spaced (axial) locations along the heated length; in essence, providing the distribution of line-averaged void along the transverse width at these thirteen locations. The measurements enable, to some degree, the detection of preferential phase distribution within the flow

cross-sectional area; the transverse void distributions were integral-averaged subsequently to estimate the axial profile of flow-area averaged void. Measurements were reported for over ten different loop-operating conditions covering a broad range of system pressure, applied heat flux, inlet subcooling and flow rate. This study considers Case 10, which represents the run with the most appreciable subcooled boiling length at high pressure. The experimental conditions for this Case are detailed in Figure 1.

### 3. The Computational Model

The practical modelling of diabatic (boiling) turbulent bubbly two-phase flow in CFD is founded on the Euler-Euler framework of interpenetrating continua, which is referred to more commonly as the two-fluid model. Within this framework, phase-averaged forms of the governing equations of conservation are solved iteratively in order to quantify the degree of non-equilibrium within the flow; that is, the pressure, velocity and temperature of each phase at each node of the computational mesh, from which the spatial distribution of phase fraction can then be extracted. A large number of constitutive relations must be specified to provide mathematical closure to this set of equations; indeed, many of the relations themselves require internal closure. At the highest level, relationships are required for determining the Reynolds stress tensor of each phase and the various interfacial exchanges (appearing as ‘source’ and ‘sink’ terms within the governing equations) of heat, mass and momentum. The relevant governing equations and associated constitutive relations have been reviewed thoroughly in a number of earlier works [4, 8, 9] and will not be discussed in great detail herein. This section serves instead to provide a general overview of the applied CFD modelling. Unless stated otherwise, the implementation of all of the specified models utilized the default code configuration. A comprehensive description of the modelling, including details of the relevant multiphase solvers and the values of all of the various modelling parameters employed may be found in the code user guide [10].

#### 3.1. Turbulence Modelling

The present investigation evaluates two broad approaches for modelling the turbulence of the (continuous) liquid phase. For the baseline solution, a standard k-epsilon model is utilized. This approach is based on the Boussinesq assumption of linear eddy viscosity and solves transport equations for the production of the turbulent kinetic energy  $k$  and its dissipation rate  $\varepsilon$  respectively, from which the Reynolds stresses may be computed indirectly as shown (assuming incompressible flow).

$$\mathbf{R} = C_{\mu} \frac{k^2}{\varepsilon} \left( \nabla \mathbf{u}_c + (\nabla \mathbf{u}_c)^T \right) - \frac{2}{3} k \mathbf{I} \quad (1)$$

Although the standard  $k$ - $\varepsilon$  model remains the most widely used approach to modelling turbulence, it still relies on an assumption of isotropic turbulent viscosity. This renders it unable to predict gradients in the normal Reynolds stresses, whose anisotropy can drive so-called ‘secondary’ (or cross-stream) flows in non-circular geometries. Whilst secondary flows are often so weak as to be negligible in single-phase calculations, and are usually overlooked, they may affect significant turbophoresis in multiphase flows [3]. Other non-linear variants of the  $k$ - $\varepsilon$  model that may offer the potential to better capture turbulence anisotropy are not applied in the present work. Instead, the more direct approach offered by Reynolds Stress Transport modelling (RSTM) is applied, wherein the notion of an eddy viscosity is discarded. This involves solving transport equations for each of the six asymmetric components of the Reynolds stress tensor, and an additional transport equation for the turbulent dissipation rate. Two RSTM variants were applied: the linear pressure-strain model of Gibson and Launder [11] and the more modern quadratic pressure-strain model of Sarkar et al. [12]. All of the applied models adopted a high-Reynolds approach. Owing to the much lower density of the (dispersed) vapor phase, it was assumed that the vapor phase turbulence could reasonably be scaled from velocity fluctuations in the liquid phase using the Issa



The partitioning model assumes a boiling area fraction  $A_b$  to split the applied heat into boiling-affected and unaffected areas, which are then used to scale the quenching and convective components respectively. The convective heat flux components are otherwise calculated in much the same way as for a normal single-phase heated flow, where the heat transfer coefficient is obtained using a characteristic temperature based on single-phase temperature wall treatments and is evaluated at the centroid of the near-wall cell. The quenching heat flux component is modelled using the approach of Del Valle and Kenning [15], who represent the process as a transient conduction into a semi-infinite medium of fluid at a uniform initial temperature. The temperature of the liquid drawn to the wall during the process of quenching is expected to be physically different to that which affects normal convection at the wall and is extracted at a constant wall  $y^+$  of 250. The evaporative heat flux component is modelled as the product of the mass flux of the departing bubble population and the latent heat of vaporization.

The partitioning model relies most heavily on three sub-models to achieve closure: these are the active nucleation site density  $N_a$ , the bubble departure diameter  $D_d$  and the bubble departure frequency  $f_d$ . The modelling of the site density and departure diameter terms is of particular importance. The former is required in the evaluation of the boiling area fraction and evaporative heat (and mass) flux component and is also strongly coupled to the wall temperature, which is the formal solved output of the overall model. The evaporative heat flux component exhibits cubic dependence on the latter, whilst the convective and quenching components both exhibit square dependence via the boiling area fraction. The departure diameter may also be used as a source term for evaluating the interfacial area in the bulk, as will be discussed. In the current work, the performance of two popular combinations of site density and departure diameter models is assessed: the Lemmert and Chawla [16] and Tolubinsky and Konstanchuk [17] models and the more advanced Hibiki and Ishii [18] and Kocamustafaogullari [19] models respectively. The expression of Cole [20] is used to define the departure frequency.

### 3.2.2. Liquid-Vapor Heat and Mass Transfer

In order to compute interphase exchanges of heat and mass as well as momentum away from the wall boundary, models are first needed to define a phasic characteristic length scale and an interfacial (or interaction) area density. A length scale is required to evaluate various non-dimensional numbers of heat, mass or momentum transfer relevance whilst the interfacial area density characterizes the area over which these transfers act. The Sauter (spherical-equivalent) bubble diameter  $d_s$  provides a convenient length scale for bubbly boiling flows. Corrections accounting for non-sphericity may be integrated separately in the exchange terms. The present work considers two approaches for obtaining the bubble size distribution.

The first and simplest approach is based on the correlation of Kurul and Podowski [14, 21] who scaled the bubble diameter linearly between two pre-defined limits according to the local liquid subcooling. The interfacial area density  $a_{cd}$  is then obtained from the computed bubble diameter using a symmetric model that incorporates the influence of the continuous phase.

$$d_s = \frac{d_{\min}(\Delta T_{sub} - \Delta T_{d,\min}) + d_{\max}(\Delta T_{d,\max} - \Delta T_{sub})}{(\Delta T_{d,\max} - \Delta T_{d,\min})} \quad (5)$$

$$a_{cd} = \frac{6\alpha_C \alpha_D}{d_s} \quad (6)$$

Through its parametric dependency on the liquid subcooling, the Kurul and Podowski length scale accounts, to an approximation, for the impact of condensation and evaporation on the Sauter bubble diameter. However, the diameter is also affected by shear and turbulence-driven breakup and coalescence.

The second applied approach accounts for this additional influence and is based on the S-Gamma ( $S_\gamma$ ) Method of Moments formulation of Lo and Rao [22], where  $S_\gamma$  represents a generalized parameter for the bubble size distribution. A pre-defined log-normal-shaped distribution of bubble sizes is assumed via the probability density function  $P(d)$ . In the present work, a one-equation approach is applied, which involves solving directly for the second moment  $S_2$  of this distribution (which is directly related to the interfacial area density) via a separate transport equation; the Sauter diameter is then calculated through Equation 6.

$$S_2 = nM_2 = \frac{a_{cd}}{\pi} = \int_0^\infty nd^2P(d)d(d) \quad (7)$$

$$\frac{1}{\pi} \left( \frac{\partial a_{cd}}{\partial t} + \nabla \cdot (\mathbf{u}_d a_{cd}) \right) = s_{break} + s_{coal} + s_{mass} + s_{wall-boil} \quad (8)$$

$$s_{wb} = N_a D_d^2 f_d \quad (9)$$

The right hand side of Equation 8 describes the various source terms for break-up, coalescence and mass transfer due to bulk evaporation/condensation as well as wall boiling. The latter term  $s_{wall-boil}$  couples the predicted bubble size distribution with core outputs from the wall heat flux partitioning, and is most dependent on the predicted value of the bubble departure diameter.

Having defined the necessary length scales, heat transfer from the liquid to the vapor-liquid interface (or vice versa) in the bulk is computed using the well-known Ranz-Marshall [23] correlation. For a subcooled flow, this will be associated with vapor condensation. A constant Nusselt number of 26 is specified to describe heat transfer between the vapor-liquid interface and the bulk steam; the exact value is not critical as any vapor formed is expected to be saturated or very near saturation. Rates of interfacial mass transfer may be calculated subsequently from the computed interfacial heat transfer terms, given that almost all of the heat transferred across the vapor-liquid interface is associated with condensation or evaporation.

### 3.2.3. Momentum Transfer

Many forces associated with phase momentum exchange may be incorporated into the modelling treatment, as illustrated in Figure 2. From a physical standpoint, the applicability and relevance of many of the non-drag forces (particularly lift and wall lubrication) under high-pressure boiling conditions is speculative and further research along these lines is required [1, 9]. Moreover, the contribution of both drag and non-drag forces at high pressure is expected to be minimal owing to the small and round bubbles anticipated. Given the aforementioned, as well as the impetus of the present study, only the simplest and least uncertain forces are considered: these are the drag force and the turbulent dispersion force. The drag coefficient was obtained using the Tomiyama model [24] whilst the dispersion force model took a logarithmic form that employed a constant turbulent Prandtl number of 1. An anisotropic approximation of the dispersion tensor diffusivity coefficient was used for combinations that involved Reynolds-stress modelling of the liquid phase turbulence.

## 3.2. Test Matrix

Following the above, the six modelling combinations outlined in Table I were investigated. Turbulence modelling was expected to play a significant role given the non-circular geometry and was examined in the first instance. Subsequent simulations that investigated the influence of wall-boiling & IAT modelling were carried out with the best-performing turbulence model identified in the first part of the study.

**Table I. Modelling combinations investigated in the present paper**

Variant	Liquid Phase Turbulence	Nucleation Site Density	Bubble Departure Diameter	Bubble Size Distribution / IAT
<b>Influence of Turbulence Modelling</b>				
V1 (Baseline)	Standard k-epsilon	Lemmert & Chawla	Tolubinsky & Konstanchuk	Kurul & Podowski
V2	RSTM (Linear Pressure Strain)	Lemmert & Chawla	Tolubinsky & Konstanchuk	Kurul & Podowski
V3	RSTM (Quadratic Pressure Strain)	Lemmert & Chawla	Tolubinsky & Konstanchuk	Kurul & Podowski
<b>Influence of Wall Heat Flux Partitioning and IAT Modelling</b>				
V4	RSTM (Linear Pressure Strain)	Lemmert & Chawla	Tolubinsky & Konstanchuk	S-Gamma
V5	RSTM (Linear Pressure Strain)	Hibiki & Ishii	Kocamustafaogullari	Kurul & Podowski
V6	RSTM (Linear Pressure Strain)	Hibiki & Ishii	Kocamustafaogullari	S-Gamma

#### 4. Simulation Methodology

Simulations were undertaken using the steady segregated solver in Version 9.04 of the commercial CFD code STAR-CCM+. The applied mesh assumed a three-dimensional coarse uniform structured nodalization scheme and comprised a quarter of the total cross-sectional area of the channel; where symmetry was assumed along the flow-exposed boundaries. A constant cross-sectional node aspect ratio of 4 was assumed, matching the aspect ratio of the channel to be simulated. The channel entrance was specified as a velocity inlet boundary whilst a static pressure outlet characterized the channel exit. Only the heated length of the channel was simulated; as such, a constant heat flux boundary condition was applied along the walls and zero heat losses from the equipment were assumed.

Given the long length (0.93 m,  $L/D_{hyd} \sim 50$ ) of the channel prior to the 1.26 m heated length, it was reasonable to expect fully developed turbulent liquid inflow conditions. In order to specify these conditions, separate single-phase adiabatic (isothermal) simulations for each applied turbulence model were carried out at the system pressure, temperature and mass flow rate. A key difference in the applied modelling for the single-phase case involved the use of an all  $y^+$  wall treatment, rather than the high  $y^+$  treatment employed for the boiling simulations (the latter being a well-known limitation of simulating diabatic flows). This enabled a more reliable estimate of the expected secondary flow behaviour at the inlet of the heated section. For convenience, these simulations were run using the same 1.26 m long quarter-symmetrical structured mesh as was used for the multiphase simulations, however the nodalization employed was substantially different owing to the dissimilar near-wall treatment. The single-phase simulations assumed a non-uniform hyperbolic nodalization scheme that enabled substantially denser refinement in the wall regions; a wall  $y^+$  of 1 - 2 was later verified during the simulations. Following a mesh convergence analysis, which also confirmed that the elected channel length achieved fully developed flow, an 80x20x250 mesh was used to carry out all of the required single-phase simulations. The velocity ( $u$ ,  $v$ ,  $w$ ) components and pertinent turbulence properties for the applied turbulence model were extracted at the outlet and imposed, subsequently, as inlet conditions for the two-phase simulations.

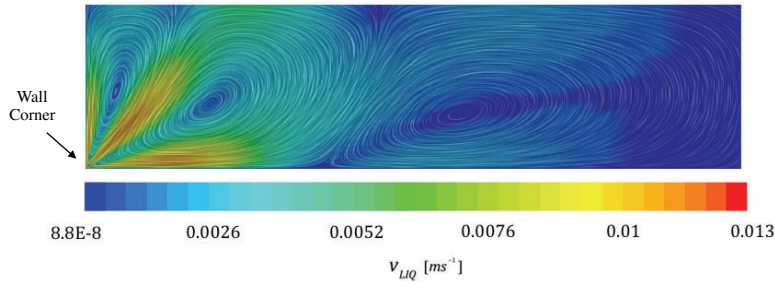


**Fig 3. The inlet cross-stream velocity distribution for the RSTM (Linear) two-phase simulations**

For simplicity, constant thermodynamic properties were assumed for both phases. Interfacial properties such as the surface tension and latent heat were also assumed to be constant. These were also reasonable assumptions given the high pressure, the low subcooling and the fact that DNB was not detected in the experiments (i.e. the vapor remains at or near saturation). The liquid properties were obtained at an intermediate subcooling of 3.5 K, taking care to match the experimental inlet mass flux, whilst vapor properties were obtained at saturation. Solver convergence was judged carefully using a range of figures of merit beyond the absolute residuals (max  $\sim 10^{-4}$ ) and measured scalars of interest: amongst others, these included monitoring global mass and heat balances, the pressure drop, the corner void fraction, wall superheat as well as the bubble size distribution at multiple locations.

## 5. Results and Discussion

### 5.1. Mesh Convergence

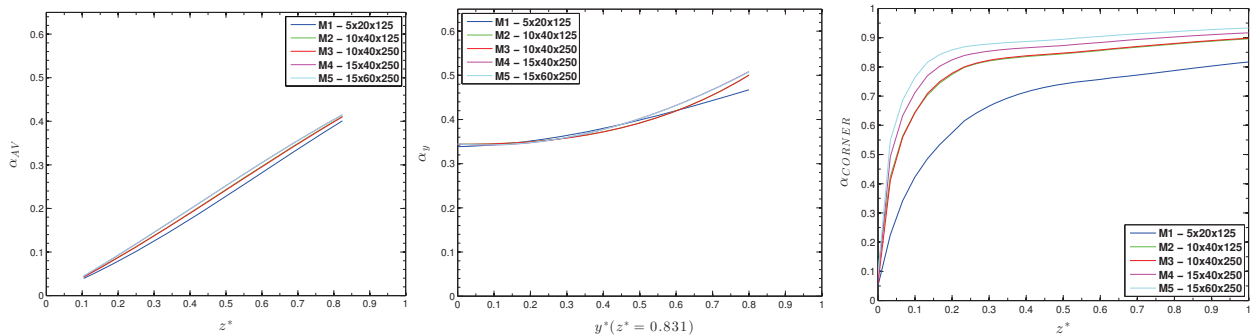


**Fig 4. Mesh convergence analyses for the baseline case (V1)**

The baseline model, which employs the simplest modelling treatment outlined in Table 1, was selected to verify mesh insensitivity. Even the coarsest mesh M1, with only 5 cells along the transverse width (and which did not facilitate the most accurate interpolation of the inlet conditions) produced plausible results for the area-averaged void and transverse void distribution. Quadrupling the cross-sectional resolution (M2) had little effect on the area-averaged void, but had a much more observable impact on the transverse void distribution, particularly closer to the wall. The void fraction in the centroid of the wall-corner cell now approached the dryout criterion at the channel exit; indeed, even the coarsest mesh predicted a maximum corner void fraction of 0.82, though the predicted wall superheats in both cases remained reasonable. A higher void fraction in the corner is anticipated given the increased density of applied heat and shear in this region. On the other hand, measurements of the outside-wall temperature were monitored during the experiment, and whilst these are not described in great detail (e.g. the exact thermocouple placement is not indicated), it is nevertheless sensible to assume that any associated excursion in wall temperature would have been detected and reported.

The predicted void fraction at any point along the wall depends on several interrelated and competing physical processes, including the formation and growth (and condensation) of bubbles at the wall and their ensuing migration towards the bulk. In the present case, void over-prediction in the corner appears to be driven, in particular, by the strong mesh sensitivity of the wall boiling formulation, which is only strictly valid when the first grid cell covers the full boundary layer thickness. The low subcooling of the investigated case and the use of the subcooling-dependent Tolubinsky-Konstanchuk diameter model may further exacerbate this sensitivity. The conservative implementation of momentum exchange terms and basic turbulence modelling applied also play a role, although it is difficult to speculate the extent to which this is the case without further investigation. With further cross-sectional refinement (M4 and M5) the corner-void along the channel exceeded the dryout criterion. Convergence was also less satisfactory for these cases; these meshes were excluded from further consideration.

Doubling the axial resolution (M3) resulted in only marginal improvement of the transverse void distributions. Nonetheless, this mesh (10x40x250) was deemed to be mesh-independent, to the extent achievable, and provided a good compromise between numerical accuracy and computational demand; all subsequent simulations were carried out on this mesh. The mesh predicted minimum and maximum wall  $y^+$  values of 40 and 300 respectively. A similar range was verified in successive simulations to ensure the applicability of the elected high Reynolds approach.

## 5.2. Influence of Turbulence Modelling

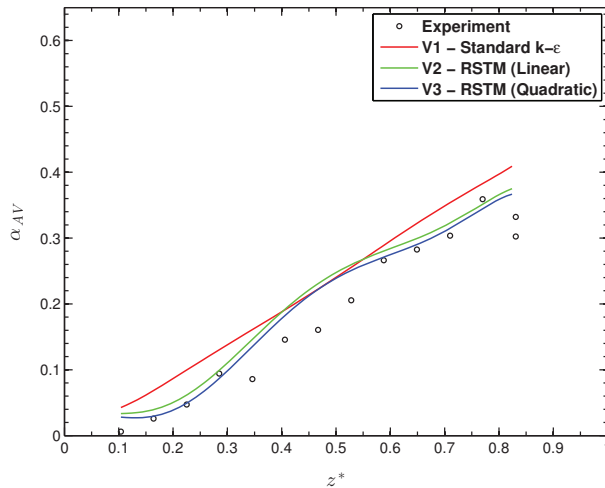


**Fig 5. Axial evolution of area-averaged void with different turbulence models**

Good overall quantitative agreement of the area-averaged void is observed with both the Linear and Quadratic Pressure-Strain RSTM variants (V2 & V3) whilst the standard  $k-\epsilon$  model (V1) generated systematic over-predictions across the entirety of the channel length. Qualitatively, the  $k-\epsilon$  model also predicted a pseudo-linear increase in the void that did not reflect the observed experimental trends. On the other hand, both RSTM variants reproduced, partially, the gradual rise in void near the channel entrance, the subsequent rapid rise in void following the onset of significant void ( $\sim z^* = 0.35$ ) and the slow plateauing of the void near the channel exit. Quantitative agreement was particularly remarkable in the entrance and exit regions ( $z^* = 0 - 0.30$  &  $z^* = 0.60 - 0.83$ ), where the experimental measurements were replicated precisely. The overshoot in the center region extended up to a deviation of 37 % and was comparable to the predictions of the  $k-\epsilon$  model. It is worth noting that one of the experimental measurements indicated a sharp drop in the averaged void at the final measurement point at  $z^* = 0.83$ , which was not captured by any model, however this was assumed to be attributable to experimental error.

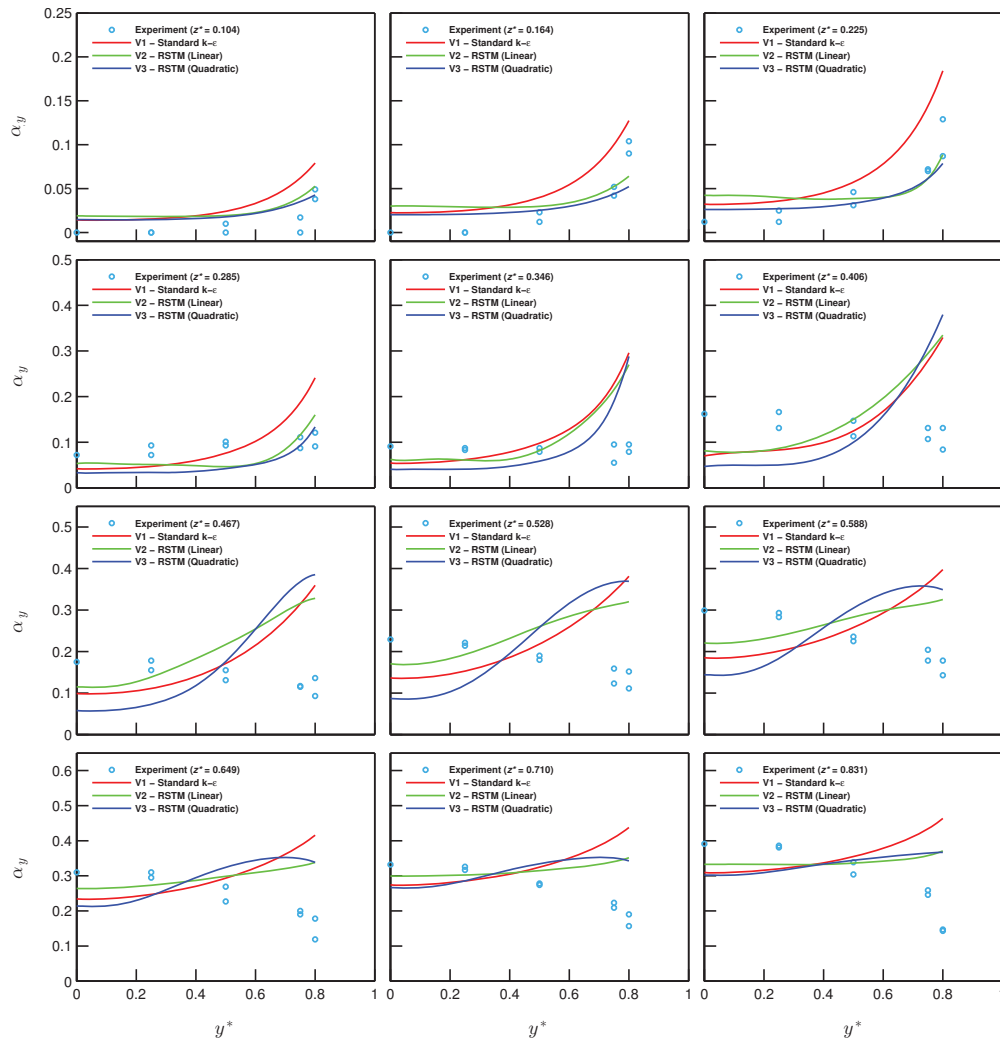


**Fig 6. Axial evolution of transverse void with different turbulence models**

An examination of the distribution of transverse averaged void, which was used to reconstruct the area-averaged void, provides a detailed picture of the phase distribution along the heated length. The measurements indicate that the migration of bubbles in the transverse direction (towards the core at  $y^* = 0$ ) is inhibited near the entrance, likely due to the flow subcooling, resulting in a void-peak near the wall and a concave-shaped void profile across the transverse width. This trend is reversed as the flow approaches saturation and vapor begins to persist in the bulk, resulting instead in a core-peak and a convex-shaped void profile. The concave-convex transition was reported to occur only a short length down the channel for the present case ( $z^* = 0.35$ ), owing presumably to the low inlet subcooling.

Both RSTM variants exhibited reasonable agreement with the measured void distributions up to  $z^* = 0.29$ , before the reported transition point. However, none of the applied models were able to capture the reported transition downstream of this point. Only the RSTM variants showed some indication of reproducing the convex core-peaking trend; the Linear model comes closest to replicating this trend and predicts a near-uniform distribution of void at the channel exit. The excellent quantitative agreement of the area-averaged void in the latter half of the channel is shown to be an artifact of the averaging-out of void under-predictions in the core and void over-predictions near the wall. As no experimental measurements of liquid temperature profiles or Sauter mean diameter are available, the exact cause of the over-shoot of area-averaged void in the center region as well as the delayed concave-convex transition

cannot be pinpointed. All modelling combinations predicted a very mildly subcooled ( $\sim 1$  K) core at the final measurement point at  $z^* = 0.83$ . The contributors to modelling uncertainty here are numerous and may involve a number of components, including the modelling of turbulence, the wall heat flux partitioning, interfacial condensation, interfacial area transport and turbulent dispersion.

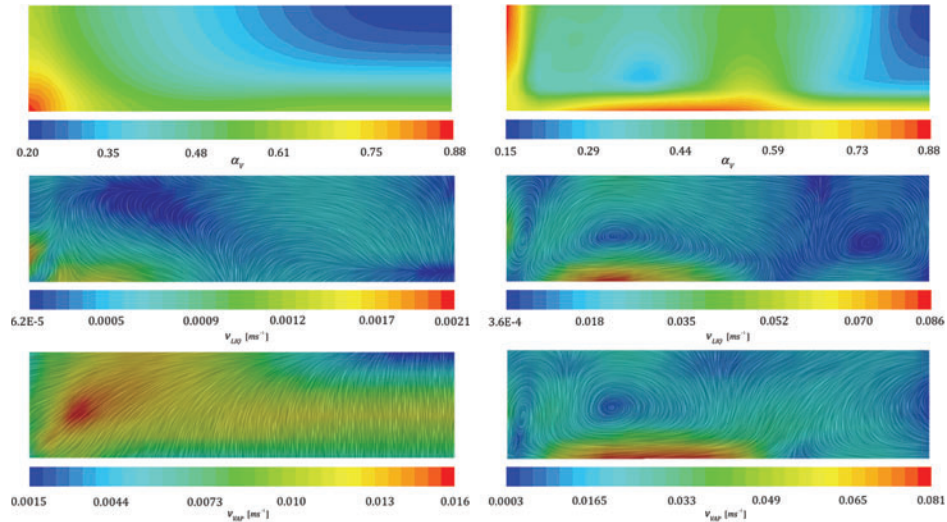


**Fig 7. Spatial void distribution and cross-stream velocities at  $z^* = 0.83$  for V1 (Left) & V2 (Right)**

It interesting to remark upon on the vastly different local void distributions predicted between the different turbulence models; these cannot be inferred by the transverse void distributions reported in Figure 6 owing to the averaging involved in the measurements. The RSTM variants, which capture the anisotropy-driven recirculation patterns in the wall-corner, suggest that secondary flows play an important role in entraining and redistributing vapor away from the corner region, along the walls and into the bulk, wherein the local void fraction exhibits a dual-peaked profile along the transverse edge and near the center of the wall. These flows might also influence the location of void-peak transition, as sustained boiling along the channel accelerates the near-wall liquid and increases the importance of these flows; the maximum secondary velocities are shown to increase from an order of 1 % of the bulk stream-wise velocity at the entrance to an order of 6 – 7 % at the channel exit. Indeed, the onset of high near-wall void ( $\alpha \sim 0.8$ ) is shifted to a normalized axial position of 0.6 compared with 0.3 for the k- $\epsilon$  model. On the other hand, the maximum near-wall void predicted within the test section remains comparable to that predicted with the k- $\epsilon$  model. Additionally, both the k- $\epsilon$  and RSTM variants suggested larger values of transverse averaged void very close to the wall ( $y^* > 0.9$ ), however the reported measurements only extend up to 80% of the half-width from the centerline ( $y^* = 0.8$ ), and as such the presence of this void peak very close to the wall can neither be confirmed nor ruled out.

Having said the above, further measurements are required to draw any conclusions on the basis of the predicted secondary flow patterns and spatial void distributions. Extending the range of transverse measurements and taking additional measurements of the longitudinally-averaged void distribution may be the most practical way forward. Whilst the reduction in corner void illustrated is counter-intuitive, there have been limited reports of similar behaviour in adiabatic air-water flows in rectangular geometries [25, 26], as such this behaviour may form part of a temporary flow regime. The prediction of the secondary vortices are also constrained and distorted by the coarse meshing requirements of the simulation and also potentially by the implementation of a turbulence response model for the vapor phase. Additionally, the turbulence introduced by the bubbles themselves has not been considered in the present framework and requires further consideration. Successive simulations applied the RST (Linear) model, whose predictions were comparable with the Quadratic variant but which offered stronger convergence.

### 5.3. Influence of Wall Boiling and IAT Modelling

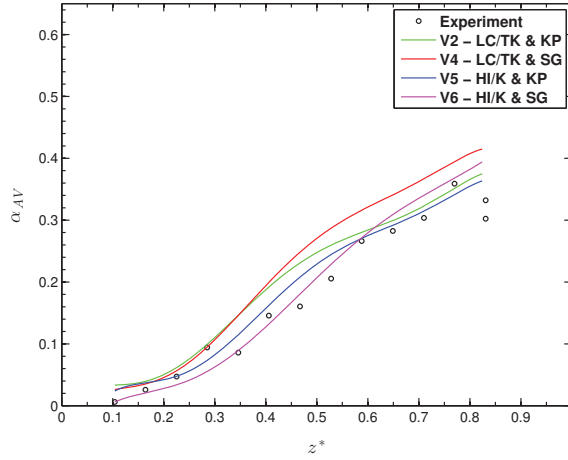


Fig 8. Axial evolution of averaged void with different combinations of wall boiling and IAT models

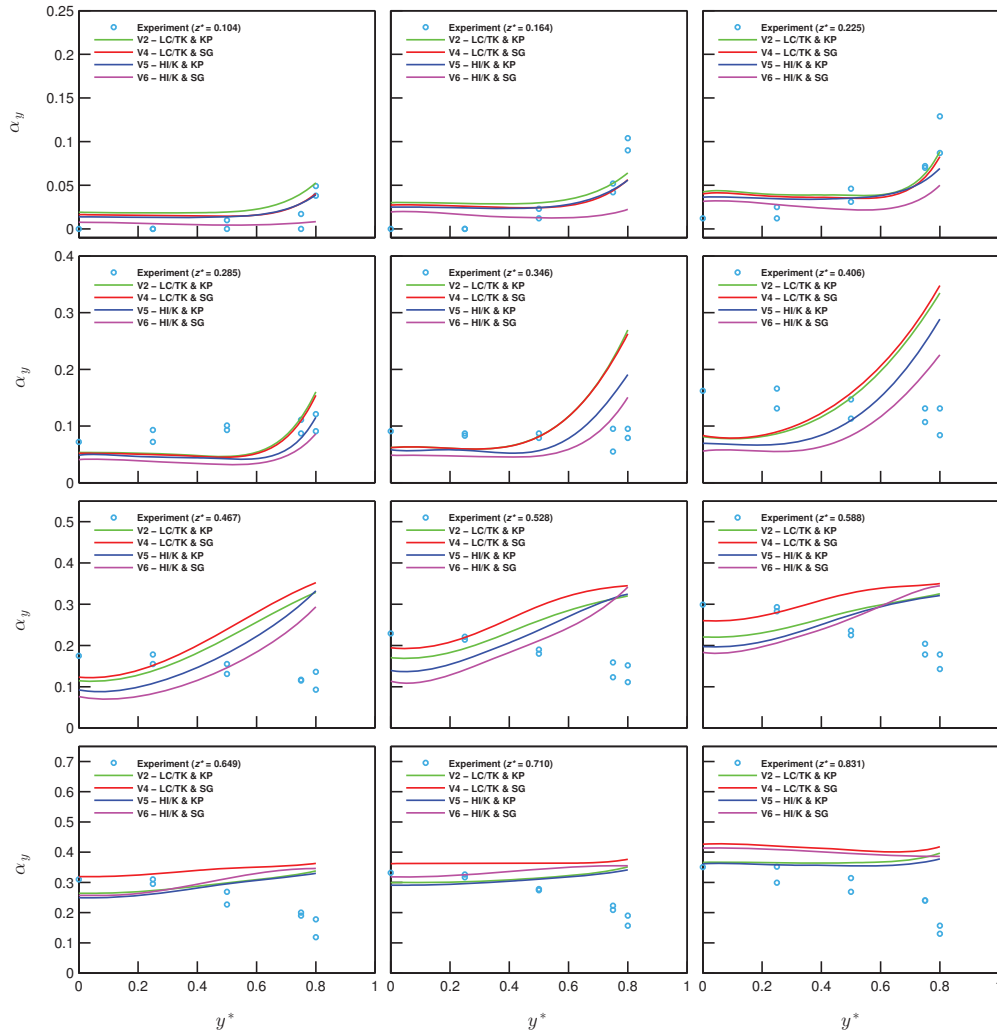


Fig 9. Axial evolution of transverse void with different combinations of wall boiling and IAT models

Following the specification of turbulence model, Figure 8 shows that the adoption of more mechanistic approaches towards wall boiling and IAT modelling may enable better agreement with the area-averaged void. However, the importance of careful pairing between the core outputs of the wall heat flux partitioning approach and IAT model is also exemplified. For instance, introducing the  $S_\gamma$  model with the existing Lemmert-Chawla/Tolubinsky-Konstanchuk (V4) partitioning actually results in significant over-predictions of the area-averaged void. This is driven chiefly by the large departure diameters ( $\sim 1$  mm) predicted by the Tolubinsky-Konstanchuk model, which is now coupled more directly with the Sauter mean diameter in the bulk and drives lower condensation rates in the flow interior. The strong sensitivity of the bulk void to the computed departure diameter has been demonstrated in recent works [27]. The best results were obtained using the Hibiki-Ishii/Kocamustafaogullari ( $D_d \sim 0.1$  mm) models in combination with the  $S_\gamma$  model, which displayed excellent overall fit with the area-averaged void. Despite the better predictions of area-averaged void, predictions of the transverse void distributions did not yield significant improvement from the baseline case, although the trend of reducing void was captured marginally better with the  $S_\gamma$  model by the end of the channel. It is again difficult to corroborate where the source of modelling uncertainty lies due to the general lack of measurements available for high-pressure flows. Nonetheless, it is reasonable to assume that significant error cancellation is involved in the predictions, especially within the wall boiling model which has been shown to be prone to this behaviour [28, 29].

## 6. Conclusions

Several configurations of the commercial CFD-code STAR-CCM+ were assessed against the measured behaviour for a high-pressure subcooled boiling flow in a rectangular geometry. The most mechanistic configurations produced remarkably good agreement with measurements of the area-averaged void. Excellent agreement was observed for the transverse distributions of line-averaged void, however this agreement was limited to the entrance of the channel. Predictions of the transverse void distributions downstream of the entrance were less satisfactory, and the transition from wall void-peak to core void-peak could not be adequately captured with any modelling configuration. The validation activity was limited by a lack of experimental data; profiles of liquid temperature, interfacial area concentration and axial and cross-stream velocity fields at elevated pressure are highly desirable. Several modelling components governing the transverse distribution of vapor could benefit from further research. These include investigating the sensitivity to interfacial forces including the lift, wall lubrication, virtual mass and turbulent dispersion forces, as well as the impact of bubble-induced turbulence. A sensitivity analysis of the break-up and coalescence mechanisms that control the predicted bubble size would be of additional benefit. The coarse meshing requirements of the wall-boiling model also impede the accurate modelling of turbulence, which may have a sizable impact in non-circular geometries owing to the presence of secondary flows; it might therefore be worthwhile to explore less grid-dependent implementations of the wall-boiling treatment and their interaction with low-Reynolds approaches in non-circular geometries.

## ACKNOWLEDGMENTS

The authors acknowledge various technical discussions with Dr. Andrew Splawski and Dr. Simon Lo, of CD-adapco. Financial support from the EPSRC and Rolls-Royce plc is also acknowledged.

## REFERENCES

- [1] Krepper, E., Končar, B., and Egorov, Y., "CFD Modelling of Subcooled Boiling - Concept, Validation and Application to Fuel Assembly Design," *Nucl. Eng. Des.* **237**(7), pp. 716-731 (2007).
- [2] Bartolomei, G. C., and Chanturiya, V. M., "Experimental Study of True Void Fraction When Boiling Subcooled Water in Vertical Tubes," *Thermal Engineering* **14**, pp. 123-128 (1967).

- [3] Krepper, E., and Rzehak, R., "CFD Analysis of a Void Distribution Benchmark of the NUPEC PSBT Tests: Model Calibration and Influence of Turbulence Modelling," *Science and Technology of Nuclear Installations*, Article ID: 939561, (2012).
- [4] Lo, S., and Osman, J., "CFD Modeling of Boiling Flow in PSBT 5×5 Bundle," *Science and Technology of Nuclear Installations*, Article ID: 795935, (2012).
- [5] Krepper, E., and Rzehak, R., "CFD for Subcooled Flow Boiling: Simulation of DEBORA Experiments," *Nucl. Eng. Des.* **241**(9), pp. 3851-3866 (2011).
- [6] Pierre, C. C. S., and Bankoff, S. G., "Vapor Volume Profiles in Developing Two-Phase Flow," *Int. J. Heat Mass Transfer* **10**(2), pp. 237-249 (1967).
- [7] Pierre, C. C. S., *Frequency-Response Analysis of Steam Voids to Sinusoidal Power Modulation in a Thin-Walled Boiling Water Coolant Channel*, Report No. ANL-7041, Argonne National Laboratory, USA (1965).
- [8] Lo, S., Splawski, A., and Yun, B. J., "The importance of correct modeling of bubble size and condensation in prediction of sub-cooled boiling flows," *NURETH-2014*, Toronto, Canada (2011).
- [9] Končar, B., and Krepper, E., "CFD Simulation of Forced Convective Boiling in Heated Channels," *CFD4NRS*, Munich, Germany (2006).
- [10] CD-adapco, "STAR-CCM+ V9.04 User Guide," (2014).
- [11] Gibson, M. M., and Launder, B. E., "Ground Effects on Pressure Fluctuations in the Atmospheric Boundary Layer," *Journal of Fluid Mechanics* **86**(3), pp. 491-511 (1978).
- [12] Speziale, C. G., Sarkar, S., and Gatski, T. B., "Modelling the Pressure–Strain Correlation of Turbulence: An Invariant Dynamical Systems Approach," *Journal of Fluid Mechanics* **227**, pp. 245-272 (1991).
- [13] Behzadi, A., Issa, R. I., and Rusche, H., "Modelling of Dispersed Bubble and Droplet Flow at High Phase Fractions," *Chem. Eng. Sci.* **59**(4), pp. 759-770 (2004).
- [14] Kurul, N., and Podowski, M. Z., "On the Modelling of Multidimensional Effects in Boiling Channels," *ANS 27th National Heat Transfer Conference*, (1991).
- [15] Del Valle, V. H., and Kenning, D. B. R., "Subcooled Flow Boiling at High Heat Flux," *Int. J. Heat Mass Transfer*, **28**(10), pp. 1907-1920 (1985).
- [16] Lemmert, M., and Chawla, J. M., *Influence of Flow Velocity on Surface Boiling Heat Transfer*, New York and Washington: Academic Press and Hemisphere (1977).
- [17] Tolubinsky, V. I., and Konstantchuk, D. M., "Vapour Bubbles Growth Rate and Heat Transfer Intensity at Subcooled Water Boiling," *ANS 4th International Heat Transfer Conference* (1970).
- [18] Hibiki, T., and Ishii, M., "Active Nucleation Site Density in Boiling Systems," *Int. J. Heat Mass Transfer* **46**(14), pp. 2587-2601 (2003).
- [19] Kocamustafaogullari, G., "Pressure Dependence of Bubble Departure Diameter for Water," *Int. Commun. Heat Mass Transfer* **10**(6), pp. 501-509 (1983).
- [20] Cole, R., "A Photographic Study of Pool Boiling in the Region of the Critical Heat Flux," *AIChE Journal* **6**(4), pp. 533-538 (1960).
- [21] Anglart, H., Nylund, O., Kurul, N., and Podowski, M. Z., "CFD Prediction of Flow and Phase Distribution in Fuel Assemblies with Spacers," *Nucl. Eng. Des.* **177**(1-3), pp. 215-228 (1997).
- [22] Lo, S., and Rao, P., "Modelling of droplet breakup and coalescence in an oil-water pipeline," *ICMF-6*, Leipzig, Germany, (2007).
- [23] Ranz, W. E., and Marshall, W., "Evaporation from Drops," *Chem. Eng. Prog.* **3**(48), pp. 141-148 (1952).
- [24] Tomiyama, A., Tamai, H., Zun, I., and Hosokawa, S., "Transverse Migration of Single Bubbles in Simple Shear Flows," *Chem. Eng. Sci.* **57**(11), pp. 1849-1858 (2002).
- [25] Sadatomi, M., Sato, Y., and Saruwatari, S., "Two-phase flow in vertical non-circular channels," *Int. J. Multiphase Flow* **8**(6), pp. 641-655 (1982).
- [26] Ohba, K., and Yhuara, Y., *Trans. Japan Soc. Mech. Engrs.*, **48**(425) (1982).
- [27] Drzewiecki, T. J., Asher, I. M., Grunloh, T. P., Petrov, V. E., Fidkowski, K. J., Manera, A., and Downar, T. J., "Sensitivity Study of Boiling and Two-Phase Flow Models in CFD," *J. Comp. Multiphase Flow* **4**(4), pp. 411 (2012).
- [28] Thakrar, R., Murallidharan, J. S., and Walker, S. P. W., "An evaluation of the RPI model for the prediction of the wall heat flux partitioning in subcooled boiling flows", *ICONE-22*, Czech Republic (2014).
- [29] Goodheart, K., Alleborn, N., Chatelain, A., and Keheley, T., "Analysis of the Interfacial Area Transport Model for Industrial Two-Phase Boiling Flow Applications," *NURETH-15*, Pisa, Italy (2013).